Physical Communication 70 (2025) 102638

Contents lists available at ScienceDirect

Physical Communication

journal homepage: www.elsevier.com/locate/phycom

Full length article

Throughput analysis of movable antenna systems with mobility exploitation models

Pedro Candeias, Rodolfo Oliveira *

Departamento de Engenharia Electrotécnica e de Computadores, Faculdade de Ciências e Tecnologia, FCT, Universidade Nova de Lisboa, 2829-516, Caparica, Portugal
Instituto de Telecomunicações, 1049-001 Lisboa, Portugal

ARTICLE INFO

Keywords:
Movable antenna wireless systems
Antenna mobility pattern
Throughput
Performance evaluation

ABSTRACT

Movable antenna systems offer a promising approach to enhancing wireless communications by dynamically adjusting antenna positions to optimize signal reception. This paper explores the performance of a movable antenna at the receiver side considering a multi-tap propagation scenario in both Single-Input Single-Output (SISO) and Multiple-Input Multiple-Output (MIMO) systems. We introduce and evaluate four distinct mobility patterns that dictate antenna movement. The mobility patterns are part of the exploitation phase, aimed at probing the achievable capacity at different antenna locations. Additionally, we account for the time required to physically move the antenna in the system throughput, considering the worst-case scenario where the transmission is temporarily paused during the antenna motion. Our analysis assesses the performance of mobility pattern heuristics by examining their ability to balance the tradeoff between capacity gains from exploring new antenna positions and the downtime due to antenna movement. Simulation results show that specific antenna mobility patterns can achieve up to 70% of the SISO's optimal throughput or 77% of the MIMO's optimal throughput. The results reported in this paper show that simple mobility patterns more than double or triple the MIMO's or SISO's throughput compared to a scenario where the antenna remains fixed in a random position, respectively, underscoring the significant potential of the antenna mobility patterns in enhancing the MA system performance.

1. Introduction

Over recent decades, we have witnessed the transition from Single-Input Single-Output (SISO) systems towards the widespread adoption of Multiple-Input Multiple-Output (MIMO) systems, which played a crucial role in the advancements of wireless communications. Alongside MIMO, there have been numerous other significant improvements [1], including but not limited to more accurate channel estimation techniques [2], a better understanding of interference properties and its management [3], full-duplex wireless systems [4], and enhanced signal processing algorithms and network architectures, all of which have contributed to the evolution of wireless networks and the delivery of faster and reliable communications. Despite these advances, the existing communication systems still face limitations regarding the full utilization of the wireless channel spatial variation in certain areas where the transmitter and receiver are located. These limitations are associated with the fact that the antennas (or antenna arrays) have a discrete arrangement positioned in fixed locations.

To overcome these setbacks new technologies have been proposed, including but not limited to Movable Antennas (MAs) [5] and Fluid Antennas [6]. Specifically, MAs can be installed at either the transmitter or the receiver and are connected to radio frequency chains through flexible cables using stepper motors to adjust the antenna position in a certain region. This feature of the MAs enables an additional spatial degree of freedom (DoF) since it allows for real-time configuration of the wireless channel. This not only allows for better connectivity but also enhances the reliability and efficiency of communication among the devices, especially when compared to the conventional fixed-position antennas (FPA) approach [5,7]. From a mechanical perspective, MAs can achieve mobility through actuators that physically move the antennas along specific axes [8] or rotate them to dynamically adapt to changing communication conditions [5]. Alternatively, antenna arrays with mechanically adjustable structures [9] can be employed to alter their configuration as needed. On the other hand, MAs can also be realized electronically, bypassing the need for physical movement. This includes the use of dual-mode patch antennas where the phase center

* Corresponding author.
E-mail address: rado@fct.unl.pt (R. Oliveira).

https://doi.org/10.1016/j.phycom.2025.102638
Received 27 December 2024; Received in revised form 22 January 2025; Accepted 16 February 2025
Available online 3 March 2025

is dynamically shifted [10], dense array antennas where subsets of elements are selectively activated to emulate movement [11], and reconfigurable antennas that electronically adjust their radiation pattern, for example, using pin-diode-loaded parasitic elements to achieve virtual rotation [12]. These approaches are more deeply described in [13] and present trade-offs in terms of mechanical durability and implementation complexity, making the choice of the method highly dependent on the application and system requirements. The mechanical movement or electronic reconfiguration of these antennas, such as rotation, tilting, or structural adaptation, can consume substantial energy depending on their speed, precision, and frequency of adjustment. Additionally, the processing of real-time data for beamforming, alignment, or direction optimization often involves complex algorithms running on dedicated hardware, further increasing energy consumption [14]. Efficient energy management strategies, including low-power actuators, lightweight materials, and advanced power optimization algorithms, are essential to ensure the sustainability and reliability of movable antennas in energy-constrained environments.

The integration of MAs in communication systems can enhance channel conditions, improve communications reliability, and reduce latency. MAs can mitigate interference and create or reinforce Line-of-Sight (LoS) links in environments with multiple obstacles, or enable more flexible beam patterns according to the users' distribution. Despite these advantages, there are also some challenges and limitations. One of the main challenges that MA-based systems face is channel estimation [15] due to the accuracy-efficiency tradeoff, which often requires complex mapping techniques or compressed sensing techniques to reduce overhead and to cope with hardware impairments. Furthermore, another challenging question is the discovery of the optimal antenna positioning which can be a complex and intensive task, especially if channel state information (CSI) is unavailable [5].

In the last few years, there have been several advances in MA communication systems. In [5], the authors presented an overview of promising applications of MA systems and their fundamentals. Furthermore, the main challenges inherent to this approach, such as channel estimation and antenna position optimization, were highlighted and some possible solutions were mentioned. The authors compared the typical fixed-position antennas with MA-based systems, concluding that MAs can improve multiple metrics such as signal power, interference suppression, flexible beamforming, and spatial multiplexing performance. The work in [16] proposed a mechanical MA architecture and a field-response-based channel model. Additionally, the maximum channel gain achievable by a single MA, in both deterministic and stochastic channels was analyzed. In [17,18] the channel estimation problem was approached with different techniques such as compressed sensing and tensor decomposition. In [19–21], the authors have focused on MIMO systems based on MA and investigated how the covariance of the transmitted signals and the positioning of the MA at the transmitter/receiver could be optimized to enhance the channel capacity. In [22–24] multiuser communication aided by MA was investigated and the results showed that the total transmit power of the users can be reduced by taking advantage of the fact that the MAs can adjust their positioning either at the users or at the base station.

MAs have also been recently adopted in pivotal technologies proposed for future generation networks, particularly, intelligent reflecting surfaces (IRS) [25], integrated sensing and communications (ISAC) [26], and non-orthogonal multiple access (NOMA) [27]. Movable antennas can complement IRS by enabling dynamic adjustment of the line-of-sight (LOS) and non-line-of-sight (NLOS) paths to optimize the signal reflections provided by IRS [28]. By repositioning the movable antenna, the system can adapt to environmental changes and ensure the IRS operates under optimal conditions, enhancing coverage and signal strength [29]. Movable antennas can improve ISAC systems by dynamically adjusting their positions to enhance sensing accuracy and communication efficiency [30]. For example, in a scenario where both tasks need to be performed simultaneously, the antenna's mobility can help achieve better localization of targets while maintaining strong communication links, optimizing the tradeoff between sensing and data transmission [31]. Movable antennas can also facilitate NOMA by dynamically positioning themselves to improve the channel conditions of users with weaker signals [32–34]. This capability enhances the performance of successive interference cancellation (SIC) and improves the overall throughput of the NOMA system, particularly in environments with heterogeneous user distributions.

Recently, the work in [35] proposed a more complex technology, named six-dimensional movable antennas (6DMA). In 6DMA, the antenna surface can be optimized in 3D positions and 3D rotations, being more flexible to explore more positions. A hybrid approach that uses 6DMA with FPA arrays was also considered in [36]. Additionally, several works considering symbiotic radio communications and coordinated multi-point (CoMP) reception were conducted in [37,38], showing that an MA array introduces an additional spatial degree of freedom by allowing flexible adjustment of all antenna positions, resulting in a substantial performance advantage over competing benchmarks. The ability of the MA to improve security and secrecy performance was also considered in [39–41], showing significant advantages of the MA-aided system over conventional fixed-position antenna systems in improving system security.

In this paper, we conduct a performance evaluation of different antenna mobility patterns to assess their impact on the throughput of SISO and MIMO wireless communication systems when only the receiving antennas are movable. We consider that during the exploitation stage, the MAs move to specific locations to evaluate the achievable capacity, after which the receiver enters the exploration stage. During the exploration state, a node receives data at the best location identified during the exploitation phase. The contributions of this work include:

- the assumption of four mobility patterns, named solutions S_2 to S_5, that are used to compare the system capacity achieved at specific spatial positions. The knowledge about the capacity at specific positions is used to improve the throughput of the wireless system;
- a methodology to conduct multiple simulations to obtain key performance indicators, particularly the achieved throughput and the tradeoff between the exploitation and exploration stages;
- the comparison of the achieved performance, in terms of throughput and energy efficiency, when considering different numbers of spatial locations and various exploitation/exploration ratios.

To the best of our knowledge, no prior work has addressed the assumption of simple yet effective mobility patterns in receiving MAs. The novelty of this paper relies on the proposed methodology to assess how different MA mobility patterns contribute to the increase of the system's throughput.

The organization of this paper is as follows: Section 2 provides an overview of the system model. Section 3 outlines the heuristics governing the antenna mobility patterns. The evaluation of the various mobility patterns is presented in Section 4, and concluding remarks are given in Section 5.

Notations: A vector of k elements is represented in lowercase boldface type, i.e. $\mathbf{v} = [v_1, v_2, \ldots, v_k]$. Uppercase boldface symbols, $\mathbf{A} \in \mathbb{R}^{m \times n}$, denote a matrix of size $m \times n$.

2. System model

2.1. MA-enabled system

In this work, we adopt the system model proposed in [20], which considers a wireless MIMO system with N transmit antennas fixed in specific positions and M receive MAs that can move along a grid of multiple spatial positions. Taking into consideration the communication wavelength, denoted by λ, we consider that the MAs can move to the Cartesian position $[x, y]$ of the 2-dimensional grid defined

by $\mathbf{J} \in \mathbb{R}^{k_x \times k_y}$, where k_x and k_y denote the number of the fixed grid positions for each dimension x and y. We admit a regular grid, i.e., $k_x = k_y$, where the positions over each dimension are defined as $\mathbf{p_x} = \mathbf{p_y} = [-n_\lambda\lambda, (1/\delta - n_\lambda)\lambda, (2/\delta - n_\lambda)\lambda, \ldots, 0, (1/\delta)\lambda, (2/\delta)\lambda, \ldots, n_\lambda\lambda]$, with $2n_\lambda\lambda, n_\lambda \in \mathbb{Z}^+$, representing the length of each dimension, and being $\delta \in \mathbb{Z}^+$ the number of discrete points considered over the λ distance.

The positions of the fixed transmit antennas and receiving MAs can be represented by Cartesian coordinates $\mathbf{t}_n = [x_t, y_t] \in \mathbb{C}_t$ and $\mathbf{r}_m = [x_r, y_r] \in \mathbb{C}_r$, respectively. The collection of coordinates of the N transmit antennas and M MAs are denoted as $\mathbf{t}^* = [t_1, t_2, \ldots, t_N] \in \mathbb{R}^{2\times N}$ and $\mathbf{r}^* = [r_1, r_2, \ldots, r_M] \in \mathbb{R}^{2\times M}$. The channel matrix between the transmitter and the receiver is denoted as $\mathbf{H}(\mathbf{t}^*, \mathbf{r}^*) \in \mathbb{C}^{M\times N}$. The symbol $\mathbf{s}$ represents the transmit signal vector with covariance matrix defined as $\mathbf{Q} = \mathbb{E}\{\mathbf{s}\mathbf{s}^H\}$. Lastly, the received signal vector is represented by

$$\mathbf{y}(\mathbf{t}^*, \mathbf{r}^*) = \mathbf{H}(\mathbf{t}^*, \mathbf{r}^*)\mathbf{s} + \mathbf{z}, \tag{1}$$

where $\mathbf{z}$ represents the additive white Gaussian noise vector at the receiver given by $\mathbf{z} \sim \mathcal{CN}(0, \sigma^2 I_M)$. I_M denotes an identity matrix of size $M \times M$.

To calculate the power achieved in each position of the grid, we consider the received signal $\mathbf{y} \in \mathbb{C}^{M\times 1}$ and proceed to determine its absolute value. After that, we square the absolute value of each element to calculate its power. The total power is then obtained by summing up all the individual powers.

2.2. Channel model

Typically MA-enabled communication systems are assumed to operate following a far-field wireless channel model, meaning that the size of the transmit and receive region is significantly smaller than the propagation distance. As such, we might consider that for each channel path component, all the transmit and receive regions have the same Angle of Arrival (AoA), Angle of Departure (AoD), and amplitude of the complex path coefficient, while the phase varies for each different position. Specifically, in the simulations conducted the values of the AoA and AoD are static. In this work, we assume the existence of 5 signal paths and the values of AoA and AoD of each path are $[-\pi/3, -\pi/6, 0, \pi/6, \pi/3]$. In terms of notation, the elevation and azimuth AoD of the transmit path are denoted as θ_t and ϕ_t, respectively. As for the receive path, the elevation and azimuth are denoted as θ_r and ϕ_r, respectively. The number of transmit and receive paths are denoted as L_t and L_r, respectively.

The difference of the signal propagation for each pth transmit path ($p = 1, 2, \ldots, L_t$) is

$$\rho_t^p(t) = x_t \sin\left(\theta_t^p\right)\cos\left(\phi_t^p\right) + y_t \cos\left(\theta_t^p\right). \tag{2}$$

The field response vector of the transmit antenna is written as

$$\mathbf{g}(t) \triangleq [e^{j\frac{2\pi}{\lambda}\rho_t^1(t)}, e^{j\frac{2\pi}{\lambda}\rho_t^2(t)}, \ldots, e^{j\frac{2\pi}{\lambda}\rho_t^{L_t}(t)}]^{\mathrm{T}} \in \mathbb{C}^{L_t}. \tag{3}$$

When the N transmit antennas are considered, the field response matrix is given by

$$\mathbf{G}(\mathbf{t}^*) \triangleq [g(t_1), g(t_2), \ldots, g(t_N)] \in \mathbb{C}^{L_t\times N}. \tag{4}$$

In a similar way, the difference of the signal propagation distance for the q-th transmit path ($q = 1, 2, \ldots, L_r$) is

$$\rho_r^q(r) = x_r \sin\left(\theta_r^q\right)\cos\left(\phi_r^q\right) + y_r \cos\left(\theta_r^q\right), \tag{5}$$

and the field response vector of the receiving MA is given by

$$\mathbf{f}(r) \triangleq [e^{j\frac{2\pi}{\lambda}\rho_r^1(r)}, e^{j\frac{2\pi}{\lambda}\rho_r^2(r)}, \ldots, e^{j\frac{2\pi}{\lambda}\rho_r^{L_r}(r)}]^{\mathrm{T}} \in \mathbb{C}^{L_r}. \tag{6}$$

Similarly to the transmit antennas, the field response matrix that considers all the M-receiving MAs is defined as

$$\mathbf{F}(\mathbf{r}^*) \triangleq [f(r_1), f(r_2), \ldots, f(r_M)] \in \mathbb{C}^{L_r\times M}. \tag{7}$$

In scenarios where multiple antennas are used, they are positioned slightly apart to simulate a realistic antenna array. For example, when considering N transmit antennas, we admit that each antenna is separated by a distance of $\vartheta = 0.01\lambda$ along the x and y directions from its adjacent antennas. This separation affects the calculation of the field response vectors as follows

$$\mathbf{g}(\mathbf{p}) = e^{j\frac{2\pi}{\lambda}[(t(1)+(n-1)\vartheta)\sin(\theta_t(p))\cos(\phi_t(p))]} e^{j\frac{2\pi}{\lambda}[(t(2)+(n-1)\vartheta)\cos(\theta_t(p))]}, \tag{8}$$

where $t(n)$ denotes the position of the nth transmit antenna.

Similarly, for the receive antennas we have

$$\mathbf{f}(\mathbf{q}) = e^{j\frac{2\pi}{\lambda}[(r(1)+(m-1)\vartheta)\sin(\theta_r(q))\cos(\phi_r(q))]} e^{j\frac{2\pi}{\lambda}[(r(2)+(m-1)\vartheta)\cos(\theta_r(q))]}, \tag{9}$$

where $r(m)$ denotes the position of the mth receive antenna.

Moreover, the path response matrix between the origin of the transmit region and the origin of the receive region is defined as $\mathbf{\Sigma} \in \mathbb{C}^{L_r\times L_t}$. Then, the response between the pth transmit path and the q-th receive path is represented by $\mathbf{\Sigma}[q, p]$. This matrix is considered to be diagonal with $\mathbf{\Sigma}[1, 1] \sim \mathcal{CN}(0, \frac{\kappa}{(\kappa+1)})$ and $\mathbf{\Sigma}[p, p] \sim \mathcal{CN}(0, \frac{1}{(\kappa+1)(L_r-1)})$. κ represents the ratio between the average power of Line of Sight (LoS) paths and Non-Line of Sight (NLoS) paths and in this case is considered to be 1.

Therefore, the channel matrix between the transmitter and the receiver is written as

$$\mathbf{H}(\mathbf{t}^*, \mathbf{r}^*) = \mathbf{F}(\mathbf{r}^*)^{\mathrm{H}}\mathbf{\Sigma}\mathbf{G}(\mathbf{t}^*). \tag{10}$$

Each realization of (10) determines the channel gains for the multiple locations of $\mathbf{G}$, which is taken into account in (1) to compute the SNR of the received signal at the multiple locations of the grid $\mathbf{J}$.

3. Antenna mobility heuristics

In total, five solutions were considered to analyze the performance of MA-based systems. The capacity for a specific position is given by

$$C = B\log_2(1 + \varrho), \tag{11}$$

where B is assumed to be 1 Hz, and ϱ represents the SNR at the receiver. The performance achieved by these solutions assumes a worst-case scenario, where the antennas do not receive any data while in motion. As such, we designate the period during which the antennas are stationary and receiving data as the "receiving time".

3.1. Solution S_1: Blind

The first solution, S_1, uses a simple and random approach representing the performance baseline. The MAs start by randomly selecting a single location in the grid. The capacity at this location is then calculated for 100,000 different realizations of the model proposed in Section 2.1 at that location. For comparison purposes, we consider the average of the capacities computed through (11). This solution considers no mobility and allows the definition of a benchmark regarding the throughput achieved at a point without ever changing the position of the antenna. Due to the lack of related work regarding mobility in these types of systems, we cannot establish a comparison between our results and those of other authors. Therefore, this conservative approach serves as a baseline for comparison purposes.

3.2. Solution S_2: Blind random

In S_2, we first consider a realization of the model in Section 2.1. The MAs can move to 12, 24, or 36 points randomly chosen from the grid $\mathbf{J}$. It is important to note that no mechanism is implemented to avoid selecting the same point multiple times. In this approach, the total time interval considered on each simulation stage, represented by T_S, is equally divided by all points. For 12 points, this means that the MAs move to a different position and remain at that location receiving

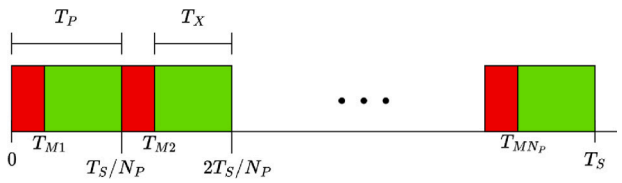

Fig. 1. Representation of T_S division for Solution S_2.

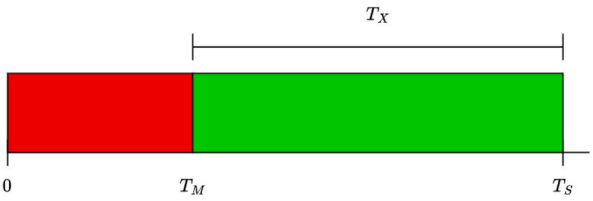

Fig. 2. Representation of T_S division for Solutions S_3, S_4 and S_5.

data for $T_S/12$ s, which includes the time needed to commute to that location, denoted as T_M. After elapsing T_S, the process is repeated considering a new realization of the model in Section 2.1 for each of the additional 999 simulation stages. This approach allows us to obtain the throughput when the antenna probes and receives data during a period on each of the considered locations, admitting that the simulation time is fairly divided by all considered locations (e.g., $T_S/12$ s per location when 12 points are considered). To better understand how the total time interval, T_S, is divided equally through all points, a visual representation is presented in Fig. 1, where $Np = 12$ represents the number of different points the antenna moves to, T_{Mx} represents the time needed to move the antenna to the xth point, T_X represents the transmission time, and $T_p = T_{Mx} + T_X$ represents the time to move to a specific point plus the time transmitting information at that point.

3.3. Solution S_3: Split phase - random

This solution is similar to the Blind Random algorithm since MAs also select random points from the grid **J** but include a constraint to prevent selecting the same point more than once. After selecting and consecutively moving to the 12, 24, or 36 points, and calculating the capacity for each, the one with the highest value is selected. Differently from the previous solution, where the MAs move to the points and the moving plus receiving time is equal to all points, in this approach, the exploitation is done first for all points, which takes a certain amount of time, T_M, due to the time required to move the antenna to the different points. Once the point with the highest capacity from the 12, 24, or 36 visited points is identified, the antenna is moved to that point and receives data during the remaining simulation time, i.e., $T_S - T_M$, identified in Fig. 2 by the green time period. Considering this approach, the antenna only receives data at the location that achieves the highest capacity, but since the visited points are randomly selected, the time spent commuting between points can eventually lower the throughput. As in solution S_2, 1000 simulation stages are performed considering independent realizations of the model in Section 2.1. A representation of the T_S division for S_3 is illustrated in Fig. 2. It is important to note that this type of structure, where the capacity of the different locations is first evaluated before the transmission stage, is also applied to solutions S_4 and S_5.

3.4. Solution S_4: Split phase - brute force

The fourth solution, S_4, is a split-phase brute force where the pattern of locations is predefined. There is a first phase of exploitation in which a first point is selected randomly and its capacity is

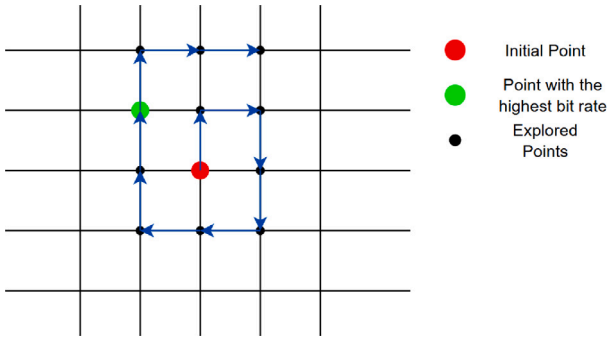

Fig. 3. Exploitation movement pattern of Solution S_4.

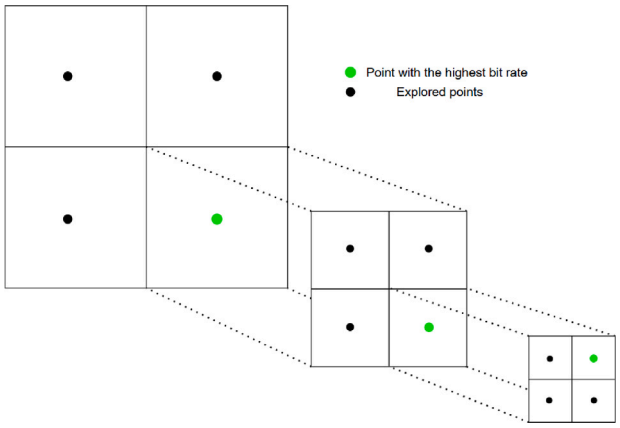

Fig. 4. Exploitation movement pattern of Solution S_5.

calculated and stored. From there, the adjacent points are traversed clockwise and their respective capacity is determined and saved as well. A representation of the described exploitation movement pattern is present in Fig. 3. When all the adjacent points are considered the radius from the initial point is increased and the points are covered clockwise once again while calculating and storing their capacity as represented by the motion pattern in Fig. 3. Once 12, 24, or 36 points are evaluated, the optimization phase begins in which the antenna is moved to the point previously identified as having the highest bit rate. This process is repeated for 999 simulation stages, considering independent realizations of the model in Section 2.1. Similarly to the previous solution, S_3, the exploitation phase is conducted at the beginning of the process and takes a certain amount of time, T_M. Then, the antenna receives data in the position in which the highest capacity was determined during the remaining time $T_S - T_M$. This approach has the upside that all the points considered are very close to each other and the commuting time T_M has a smaller influence on the final throughput when compared to S_3.

3.5. Solution S_5: Split phase - hierarchical

The last solution is also a split-phase and follows a hierarchical approach. Fig. 4 presents an illustration of how this solution is applied with regards to the subsequent division of the grid **J** in quadrants. The approach starts with the exploitation phase in which the grid is divided into four quadrants and the capacity of the center point of each quadrant is calculated. The four capacity values obtained in each quadrant are then compared and the quadrant with the highest capacity is then selected. The described process is then repeated for the selected quadrant. The quadrant is divided again, with the previously identified best point becoming the center of the new quadrants. This procedure is

Table 1
Throughput mean values and confidence intervals for different solutions and configurations - SISO scenario with $L_t = L_r = 3$.

Solution	# of points	T_S (s)	S (bps/Hz)	S - confidence int.
S_1	–	–	2.0443	[2.0344, 2.0543]
S_2	12	60	1.7862	[1.7611, 1.8114]
S_2	12	30	1.5514	[1.5292, 1.5736]
S_2	24	60	1.5199	[1.5039, 1.5359]
S_2	24	30	1.0114	[0.99932, 1.0235]
S_2	36	60	1.2735	[1.2621, 1.2849]
S_2	36	30	0.49195	[0.48222, 0.50169]
S_3	12	60	4.4803	[4.4092, 4.5514]
S_3	12	30	3.8268	[3.7659, 3.8877]
S_3	24	60	4.3488	[4.2949, 4.4027]
S_3	24	30	2.8196	[2.7796, 2.8596]
S_3	36	60	3.8471	[3.8063, 3.888]
S_3	36	30	1.356	[1.3266, 1.3855]
S_4	12	60	5.1879	[5.1071, 5.2687]
S_4	12	30	5.1656	[5.0836, 5.2476]
S_4	24	60	5.8503	[5.7809, 5.9197]
S_4	24	30	5.7219	[5.656, 5.7877]
S_4	36	60	6.225	[6.1595, 6.2905]
S_4	36	30	6.0743	[6.0149, 6.1338]
S_5	12	60	3.5391	[3.4512, 3.6269]
S_5	12	30	3.2459	[3.1652, 3.3265]

Table 2
Throughput mean values and confidence intervals for different solutions and configurations - MIMO scenarios with $L_t = L_r = 5$.

Solution	# of points	T_S (s)	S (bps/Hz)	S - confidence int.
S_1	–	–	3.945	[3.932, 3.9581]
S_2	12	60	3.4575	[3.4227, 3.4923]
S_2	12	30	2.9686	[2.9387, 2.9986]
S_2	24	60	2.9429	[2.922, 2.9638]
S_2	24	30	1.9582	[1.9396, 1.9768]
S_2	36	60	2.4406	[2.4248, 2.4564]
S_2	36	30	0.92933	[0.9121, 0.94656]
S_3	12	60	6.6237	[6.5562, 6.6911]
S_3	12	30	5.6009	[5.5404, 5.6614]
S_3	24	60	6.1738	[6.1222, 6.2255]
S_3	24	30	3.9303	[3.888, 3.9725]
S_3	36	60	5.2996	[5.2568, 5.3425]
S_3	36	30	1.8732	[1.8341, 1.9124]
S_4	12	60	7.6536	[7.5789, 7.7284]
S_4	12	30	7.534	[7.4566, 7.6114]
S_4	24	60	8.2082	[8.1432, 8.2733]
S_4	24	30	8.1458	[8.0806, 8.211]
S_4	36	60	8.5502	[8.4909, 8.6094]
S_4	36	30	8.3411	[8.2813, 8.4009]
S_5	12	60	5.7267	[5.6321, 5.8214]
S_5	12	30	5.2514	[5.1646, 5.3382]

repeated once more, changing the search area again. Due to the adopted method, this solution considers only 12 points of exploitation (4 points in each of the 3 quadrants). When the point with the highest capacity is identified, its capacity is considered for the rest of the stage simulation time (T_S). This process is repeated for additional 999 simulation stages, considering independent realizations of the model in Section 2.1. We highlight that the commuting time during the exploitation phase is considered and the antenna only receives data at the point that achieves the highest capacity during the exploitation phase. This approach is a bit more restrictive in terms of which points can be considered, which might inhibit the solution from achieving higher values of capacity. However, this restriction also means that the time spent transitioning between points is constant due to the fixed pattern of locations, which can be an advantage when compared to the random selection of the points considered in the exploitation phase of solutions S_2 and S_3.

3.6. Final remarks

In this work we do not focus on analyzing the additional computational and signaling overhead associated with real-time channel state estimation and antenna positioning. However, we acknowledge the practical significance of channel estimation and its integration into the system's operation. In the proposed solutions, we explicitly account for the time required to move the antenna, as this is a critical factor affecting system performance. Notably, the time scale of antenna movement is relatively slow compared to the time needed for channel estimation in most practical scenarios. Therefore, the time allocated for antenna movement can inherently accommodate the time required for channel state estimation without significantly impacting the overall system performance and is an important aspect of the exploitation stage in all the proposed solutions, because an accurate estimation of the channel state at each exploitation location is required to determine the capacity C achieved in that position.

4. Performance evaluation

In this section, we present the simulation results to assess the performance of the solutions proposed in Section 3. The section evaluates the throughput performance and energy efficiency.

4.1. Throughput performance

The throughput performance is evaluated through simulation. In the simulation, the transmission frequency is assumed to be 1 GHz and the wavelength (λ) is 30 cm. The grid considered has 40 × 40 discrete points, totaling 1600 points, considering $n_\lambda = 2$ and $\delta = 10$. The simulation assumes 2 different scenarios. The first scenario considers a SISO communication system with a single fixed transmit antenna at the position [0, 0] and a single MA receive antenna that moves according to the different movement patterns of the proposed solutions. In this scenario, the number of transmit and receive paths are the same, i.e., $L_t = L_r$=3. The second scenario is a MIMO communication system with 2 fixed transmit antennas in the positions [0,0] and [0+ϑ, 0+ϑ] and 2 MA receive antennas that also move according to the solutions presented in Section 3. The number of transmit and receive paths are the same, i.e., $L_t = L_r$=5. The noise is generated considering $\sigma = 1$.

In solutions S_2, S_3, and S_4, the number of exploitation points is assumed to be 12, 24, and 36. We highlight that in solution S_5 only 12 exploitation points are considered due to the hierarchic exploitation search. For the solution S_1 only a single location is considered, as the receiver is always fixed at that location. We consider two different values for the duration of each simulation stage, i.e., T_S lasts 30 s or 60 s, to assess the influence of the exploitation commuting time on the duration of the simulation stage. During the T_S period, the receiver halts the reception while commuting to a different location, and the throughput, S, considers the capacity achieved at the locations of the MAs when not moving. The throughput incorporates the amount of weighted time that MAs receive data, i.e., the capacity is weighed by

$$\frac{T_S - T_M}{T_S}, T_M < T_S,$$

where T_M represents the time commuting to the different exploitation locations. T_M is computed considering the physical distance between the transitioned points and admits that the antenna moves at a speed of 1 m/s.

The throughput values for the first and second scenarios are presented in Table 1 and Table 2, respectively, for the different solutions, number of exploitation points, simulation time, and average and confidence interval at 95% of the confidence level of the throughput.

The same results are plotted in Fig. 5 and Fig. 7 for the SISO and MIMO scenarios respectively. These figures present the maximum achievable throughput of 8.38322 bps/Hz for the SISO scenario and

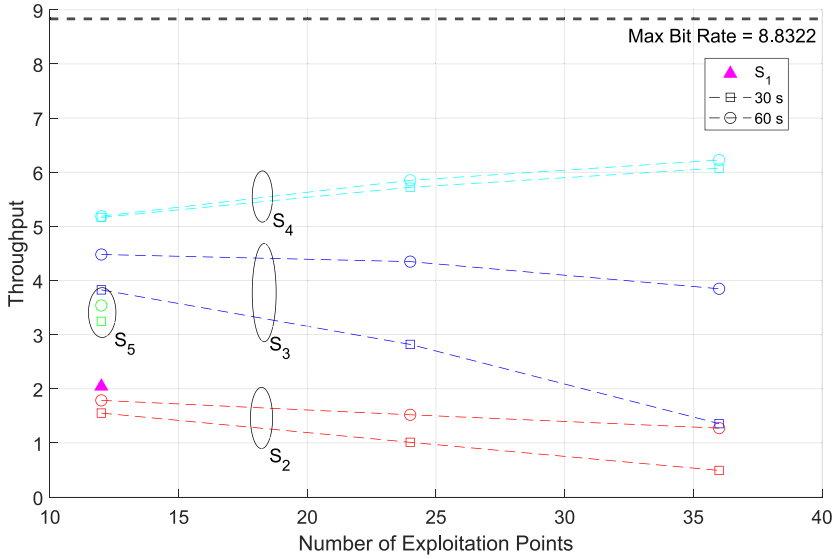

Fig. 5. Comparison of the average throughput, S (in bps/Hz), for different solutions and configurations for the SISO scenario.

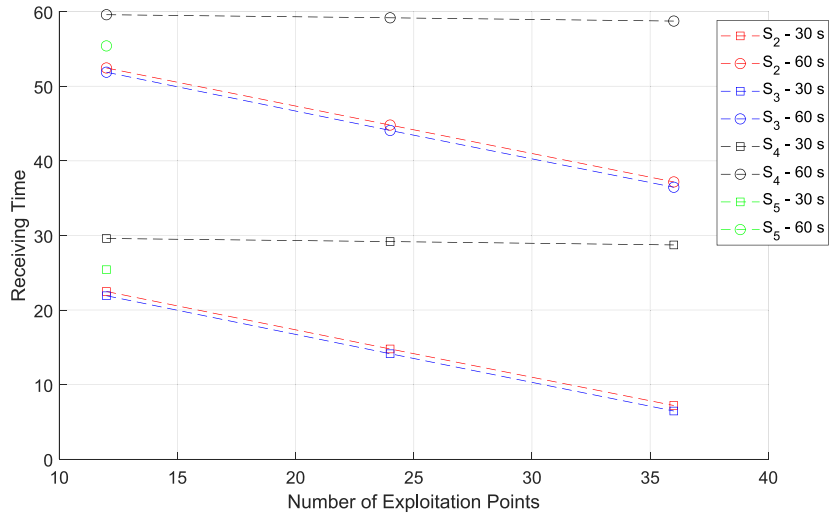

Fig. 6. Comparison of receiving time (in seconds), $T_S - T_M$, for the different solutions and configurations shown in Fig. 5.

11.1089 bps/Hz for the MIMO scenario. These maximum values were computed considering that the MAs were positioned during the entire simulation period T_S at the location of the grid where the maximum capacity is achieved and for 1000 independent realization of the model in Section 2.1.

Regarding the results plotted in Figs. 5 and 7, we observe that maintaining the MAs at a random fixed position during the entire simulation (S_1) can perform better than adopting the random exploitation points according to the solution S_2. The cause of underperformance of S_2 is mainly due to the time commuting to the multiple random locations, which limits the receiving time, as shown in Figs. 6 and 8. In S_2, the results in Fig. 6 show that the receiving time decreases as more exploitation points are considered, lowering the achieved throughput, as plotted in Fig. 5. The results regarding the MIMO scenario also show the same behavior.

When comparing solutions S_2 and S_3, we conclude that the throughput achieved by S_3 is significantly higher, showing the advantage of only starting the reception on the location that achieves the highest capacity during the exploitation stage. Although the results for both scenarios show that S_2 and S_3 achieve similar receiving times, S_3 benefits from receiving at the optimal location from the ones probed during the exploitation, which increases the throughput of the simulated scenarios of least 88%. In both S_2 and S_3, the throughput decreases if a shorter simulating stage is assumed, i.e., $T_S = 30$ s instead of $T_S = 60$ s, due to the influence of a similar commuting time in a shorter simulation stage period.

In Fig. 5, we observe that solution S_4 achieves the highest throughput. As can be seen from the results in Fig. 6, this advantage is mainly due to the low commuting time due to the proximity of the exploited locations, which allows the MAs to receive data for a longer period when compared to the other solutions. For S_4, we also observe a slight increase in the throughput with the number of exploited points, which is explained by the larger diversity of locations probed during the exploitation stage. Regarding the results achieved in S_5, the throughput is slightly lower than the throughput achieved by S_3, and although this solution achieves a higher receiving time, the mobility pattern during the exploitation stage is not so efficient as the one adopted in S_3 or S_4. Once again, the same conclusions can be drawn for the MIMO results.

We highlight that both S_3, S_4, and S_5, achieve higher throughput than a randomly chosen fixed location, as adopted in S_1, and in the best

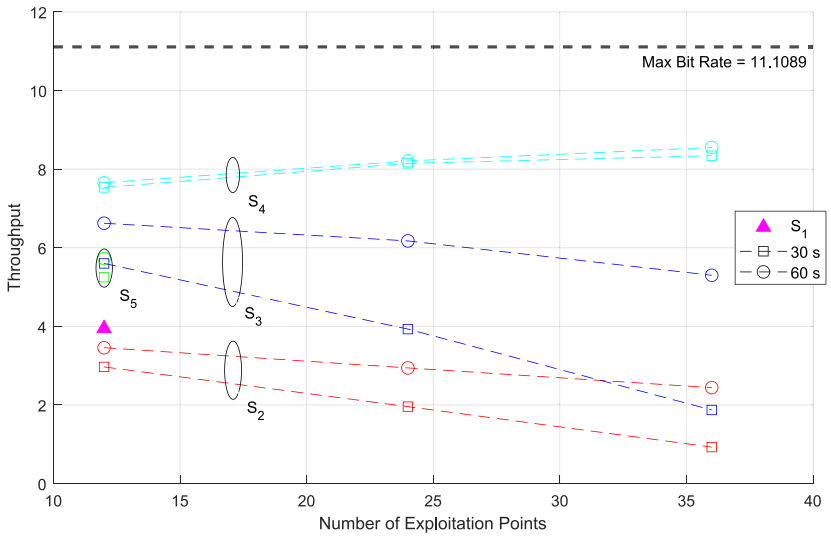

Fig. 7. Comparison of the average throughput, S (in bps/Hz), for different solutions and configurations for the MIMO scenario.

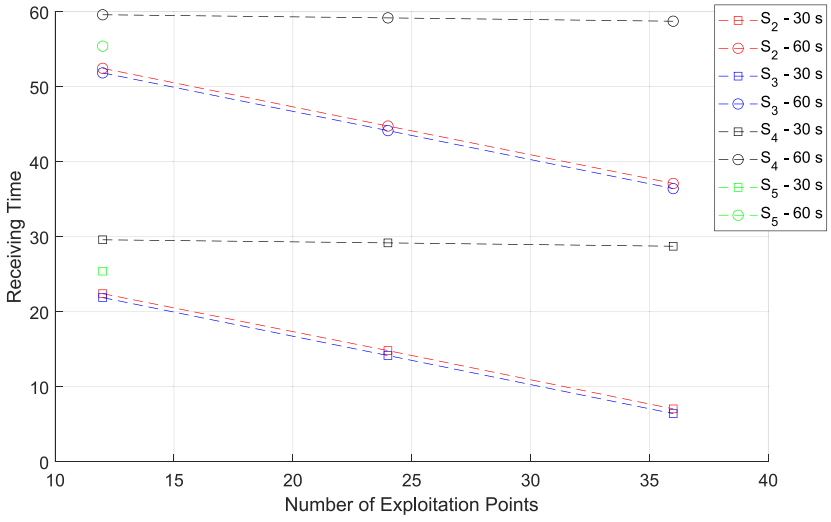

Fig. 8. Comparison of receiving time (in seconds), $T_S - T_M$, for the different solutions and configurations shown in Fig. 7.

case, the solution S_4 can effectively double the throughput achieved by S_1 and achieve approximately 77% of the optimal throughput in both cases. Additionally, we show that in our study, which considers a SISO and a MIMO scenario with different numbers of transmit paths, the trend of the performance of all the solutions is equivalent for both cases, meaning that the only advantage of a more complex system, like MIMO, and considering more transmit paths is that this system can achieve higher capacity values but it does not affect the overall performance of the proposed antenna mobility solutions.

Finally, we outline that while the proposed mobility solutions are solely focused on the motion aspect and do not inherently adapt to environmental changes such as obstacles or interference, the exploitation plus exploration time, T_S, can be shortened to enable more frequent sampling of multiple positions. By doing so, the proposed solutions can indirectly account for signal degradation at specific locations by revisiting them more often. It is important to note, however, that this approach introduces a tradeoff: on one hand, performance may improve due to more frequent exploration and adaptation to environmental conditions. On the other hand, the mobility overhead increases as a result of more frequent exploration. This tradeoff needs to be carefully evaluated based on the specific application and deployment scenario.

4.2. Energy efficiency

Energy efficiency is an important aspect of MA systems, particularly in the context of modern wireless networks where sustainability and energy conservation are key considerations. MA systems consume energy primarily for their repositioning mechanisms and data transmission. To ensure energy efficiency, it is essential to balance the energy spent on antenna movement with the gains achieved in communication performance. In our work, the mobility patterns are designed as heuristics and some of them avoid unnecessary movement, thereby reducing energy overhead while improving the communication performance.

The movement of the antenna introduces a tradeoff between the energy consumed for mobility and the potential gains in communication performance. While static antenna systems avoid mobility energy costs, they may require higher transmission power to compensate for suboptimal positioning, especially in dynamic environments. Movable antennas, by adaptively optimizing their positions, can achieve improved energy efficiency in the long run by reducing the transmission power required to maintain link quality.

We evaluate the energy consumption associated with communications and antenna mobility. The power required for communications is denoted by P_C. The power required for antenna mobility is represented

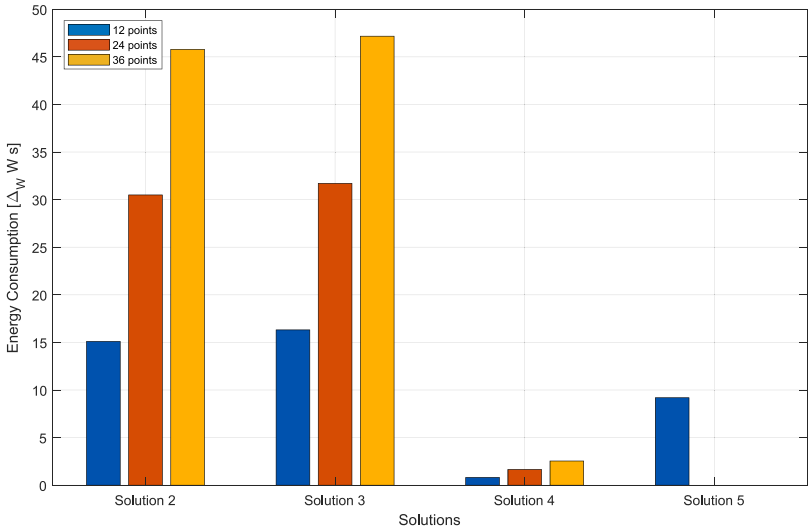

Fig. 9. Energy consumption, E_M, for the MIMO scenario considered in Fig. 7 and for $P_M = 2\Delta_W$ W and $T_S = 60$ s.

by P_M. To generalize, we consider that P_C and P_M are given in Δ_W units of power. The ratio of antenna mobility power to communication power is given by

$$\gamma = \frac{P_M}{P_C}. \tag{12}$$

The energy consumption due to communications is expressed as

$$E_C = P_C(T_S - T_M), \tag{13}$$

where T_S and T_M are the durations defined for each solution in Section 3. The energy consumption due to antenna mobility is given by

$$E_M = P_M T_M. \tag{14}$$

The energy efficiency of the system is defined as the ratio of the achievable communication capacity C to the total energy consumption $E_C + E_M$, and is written as

$$\Gamma = \frac{C}{E_C + E_M}. \tag{15}$$

This metric provides a quantitative measure of the system's ability to balance communication performance with energy usage.

The results in Fig. 9 illustrate the energy consumption due to mobility, E_M, for the MIMO scenario considered in Fig. 7, assuming that the power required for antenna mobility is $P_M = 2\Delta_W$. The results are provided for solutions 2 to 5, as solution 1 is excluded since it represents the case of a fixed antenna without mobility. Furthermore, the results include the different exploitation points adopted in solutions 2, 3, and 4. In general, it is observed that solution 3 slightly consumes more energy for antenna mobility than solution 2, whereas solution 4 achieves the lowest energy consumption. This behavior is primarily due to the closeness of the points to which the antenna moves in solution 4, which reduces the energy required for mobility.

The results in Fig. 10 illustrate the energy efficiency, Γ, for the MIMO scenario considered in Fig. 7, assuming that the power required for antenna mobility can be 2 or 4 times the power required for communication, i.e., $\gamma = 2$ or $\gamma = 4$, respectively. The results indicate that solution 2 is always less efficient than maintaining the antenna in a fixed position. This observation also holds true for solution 3 with 4 and 36 exploitation points, as the energy consumed to move the antenna strongly penalizes the energy efficiency. However, for solutions 4, 5, and solution 3 with 12 exploitation points, the gain in throughput combined with the low energy consumption due to antenna mobility makes them more energy efficient. These results show that MAs can simultaneously improve throughput and energy efficiency compared to fixed antenna solutions. Nevertheless, we emphasize the importance of selecting mobility patterns that minimize the distance the antenna must move to identify locations where capacity is effectively increased.

5. Conclusions

This paper has showed the potential benefits of using movable antenna systems to enhance the performance of SISO systems and multi-tap MIMO systems. By introducing and evaluating four distinct antenna mobility patterns, we have provided insights into how dynamic antenna positioning can improve system capacity. Our results show that by carefully selecting mobility patterns, up to 77% of the system's optimal throughput can be achieved, highlighting the importance of exploiting spatial diversity through antenna movement. Additionally, we have shown that even simple mobility patterns can significantly improve performance, more than doubling system throughput compared to a static antenna setup. However, we also acknowledged the tradeoff between throughput gains and the downtime associated with antenna movement, which needs to be carefully balanced in practical implementations. Regarding the practical feasibility of the proposed solutions, we highlight that the implementation of the different solutions requires a movable antenna system, but as simple heuristics, they do not necessitate additional hardware beyond the mobility mechanisms, resulting in no added hardware costs. Additionally, these heuristic-based solutions avoid complex optimization processes, reducing system complexity compared to optimal schemes that require extensive environmental information and computational resources. This simplicity enhances the practical feasibility of the approach, particularly in scenarios where cost-effectiveness and reduced complexity are essential.

Future research could focus on integrating movable antenna systems with advanced network architectures, such as IRS, ISAC, and NOMA. This integration has the potential to optimize coverage, capacity, and spectral efficiency, especially in 5G and beyond. Additionally, while our goal in this work is focused on predefined mobility patterns, future work could investigate adaptive mobility patterns that dynamically respond to real-time environmental factors like obstacles, interference, and user mobility. This direction would benefit from the incorporation of machine learning algorithms for environment-aware decision-making. Energy consumption remains a critical challenge, and exploring energy-efficient mobility mechanisms, along with assessing their impact on network performance, could pave the way for more sustainable deployments. Finally, extending movable antenna systems to emerging use cases, such as unmanned aerial vehicles (UAVs),

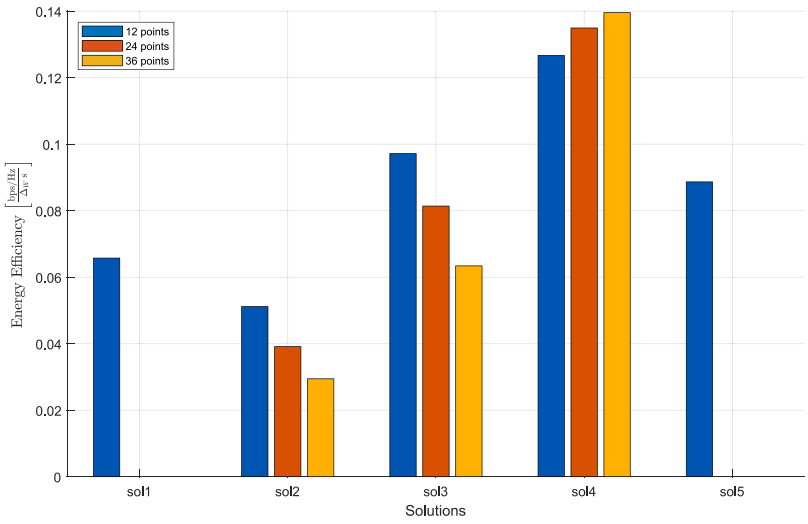

(a) $\gamma = 2$

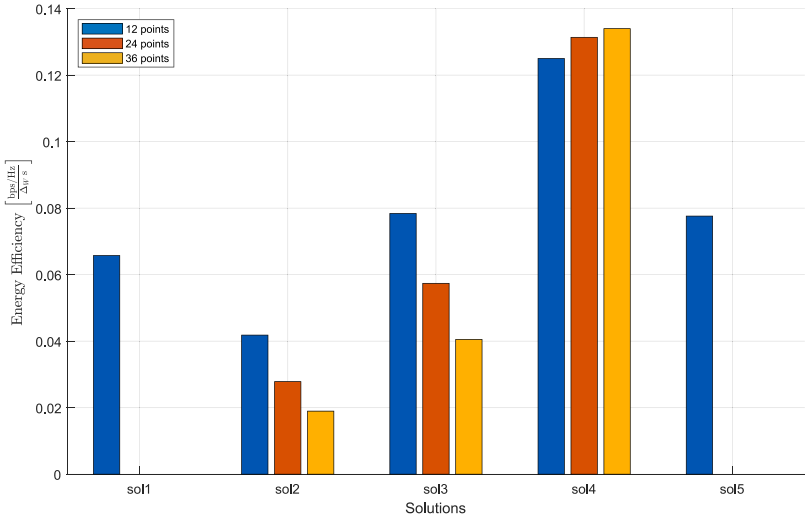

(b) $\gamma = 4$

Fig. 10. Energy efficiency, Γ, for the MIMO scenario considered in Fig. 7 and for $P_M = \Delta_W$ W, $T_S = 60$ s, and different γ values.

autonomous vehicles, and industrial IoT, where dynamic mobility is essential for reliable communications, could significantly enhance the practical applicability of these systems.

CRediT authorship contribution statement

Pedro Candeias: Writing – review & editing, Writing – original draft, Methodology, Investigation, Data curation. **Rodolfo Oliveira:** Writing – review & editing, Writing – original draft, Supervision, Methodology, Investigation.

Declaration of competing interest

The authors declare the following financial interests/personal relationships which may be considered as potential competing interests: Rodolfo Oliveira and Pedro Candeias reports financial support was provided by Foundation for Science and Technology. If there are other authors, they declare that they have no known competing financial interests or personal relationships that could have appeared to influence the work reported in this paper.

Acknowledgments

This work was supported by *Fundação para a Ciência e Tecnologia*, Portugal, by project reference UIDB/50008/2020, and DOI identifier https://doi.org/10.54499/UIDB/50008/2020, and by project reference 2022.087 86.PTDC and DOI identifier https://doi.org/10.54499/2022.08786.PTDC.

Data availability

No data was used for the research described in the article.

References

[1] E. Hossain, M. Hasan, 5G cellular: Key enabling technologies and research challenges, IEEE Instrum. Meas. Mag. (2015).

[2] R. Verdecia-Pena, R. Oliveira, J.I. Alonso, Enhancing mmwave channel estimation: A practical experimentation approach with modeled physical layer impairments incorporated in deep learning training, IEEE Open J. Commun. Soc. (2024).

[3] L. Irio, R. Oliveira, L. Bernardo, Aggregate interference in random waypoint mobile networks, IEEE Commun. Lett. (2015).
[4] A.T. Abusabah, L. Irio, R. Oliveira, D.B. da Costa, Approximate distributions of the residual self-interference power in multi-tap full-duplex systems, IEEE Wirel. Commun. Lett. (2021).
[5] L. Zhu, W. Ma, R. Zhang, Movable antennas for wireless communication: Opportunities and challenges, IEEE Commun. Mag. (2023).
[6] K.-K. Wong, A. Shojaeifard, K.-F. Tong, Y. Zhang, Fluid antenna systems, IEEE Trans. Wirel. Commun. (2021).
[7] L. Zhu, W. Ma, R. Zhang, Movable-antenna array enhanced beamforming: Achieving full array gain with null steering, IEEE Commun. Lett. (2023).
[8] S. Basbug, Design and synthesis of antenna array with movable elements along semicircular paths, IEEE Antennas Wirel. Propagat. Lett. 16 (2017) 3059–3062.
[9] L.-W. Zhao, Y.F. Wu, C. Wang, Y. Guo, A 3-d-printed deployable luneburg lens antenna based on the pop-up kirigami sphere, IEEE Trans. Antennas Propagat. 71 (8) (2023) 6481–6489.
[10] T. Mitha, M. Pour, Principles of adaptive element spacing in linear array antennas, Sci. Rep. 11 (2021) 5584.
[11] W. Mei, X. Wei, B. Ning, Z. Chen, R. Zhang, Movable-antenna position optimization: A graph-based approach, IEEE Wirel. Commun. Lett. 13 (7) (2024) 1853–1857.
[12] Z. Ding, J. Chen, H. Zhou, R. Jin, Two-dimensional scanning phased array with large element spacing using pattern reconfigurable stacked patch antenna at Ka-band, IEEE Trans. Antennas Propagat. 70 (7) (2022) 5447–5457.
[13] B. Ning, S. Yang, Y. Wu, P. Wang, W. Mei, C. Yuen, E. Björnson, Movable antenna-enhanced wireless communications: General architectures and implementation methods, 2024, arXiv.
[14] H. Wang, Q. Wu, W. Chen, Movable antenna enabled interference network: Joint antenna position and beamforming design, IEEE Wirel. Commun. Lett. 13 (9) (2024) 2517–2521.
[15] Z. Zhang, J. Zhu, L. Dai, R.W. Heath, Successive Bayesian reconstructor for channel estimation in fluid antenna systems, IEEE Trans. Wirel. Commun. (2024).
[16] L. Zhu, W. Ma, R. Zhang, Modeling and performance analysis for movable antenna enabled wireless communications, IEEE Trans. Wirel. Commun. (2023).
[17] W. Ma, L. Zhu, R. Zhang, Compressed sensing based channel estimation for movable antenna communications, IEEE Commun. Lett. 27 (2023) 2747–2751.
[18] R. Zhang, L. Cheng, W. Zhang, X. Guan, Y. Cai, W. Wu, R. Zhang, Channel estimation for movable-antenna MIMO systems via tensor decomposition, IEEE Wirel. Commun. Lett. (2024).
[19] Ma W., L. Zhu, R. Zhang, Capacity maximization for movable antenna enabled MIMO communication, in: ICC 2023 - IEEE International Conference on Communications, 2023.
[20] W. Ma, L. Zhu, R. Zhang, MIMO capacity characterization for movable antenna systems, IEEE Trans. Wirel. Commun. (2023).
[21] Chen X., B. Feng, Y. Wu, D.W.K. Ng, R. Schober, Joint beamforming and antenna movement design for moveable antenna systems based on statistical CSI, in: GLOBECOM 2023 - IEEE Global Communications Conference, 2023.
[22] Pi X., L. Zhu, Z. Xiao, R. Zhang, Multiuser communications with movable-antenna base station via antenna position optimization, in: 2023 IEEE Globecom Workshops, GC Wkshps, 2023.
[23] S. Yang, W. Lyu, B. Ning, Z. Zhang, C. Yuen, Flexible precoding for multi-user movable antenna communications, IEEE Wirel. Commun. Lett. (2024).
[24] Wu Y., D. Xu, D.W.K. Ng, W. Gerstacker, R. Schober, Movable antenna-enhanced multiuser communication: Jointly optimal discrete antenna positioning and beamforming, in: GLOBECOM 2023 - IEEE Global Communications Conference, 2023.
[25] P. Saikia, A. Jee, K. Singh, C. Pan, T.A. Tsiftsis, W.-J. Huang, RIS-aided integrated sensing and communications, in: GLOBECOM 2023-2023 IEEE Global Communications Conference, Kuala Lumpur, Malaysia, 2023.
[26] F. Liu, et al., Integrated sensing and communications: Toward dual-functional wireless networks for 6G and beyond, IEEE J. Sel. Areas Commun. 40 (6) (2022) 1728–1767.
[27] A. Jee, K. Agrawal, S. Prakriya, A coordinated direct AF/DF relay-aided NOMA framework for low outage, IEEE Trans. Commun. 70 (3) (2022) 1559–1579.
[28] B. Zhang, et al., Sum-rate enhancement for RIS-assisted movable antenna systems: Joint transmit beamforming, reflecting design, and antenna positioning, IEEE Trans. Veh. Technol. (2024).
[29] W. Xie, et al., Movable antenna-assisted covert communications with reconfigurable intelligent surfaces, IEEE Internet Things J. (2024).
[30] W. Lyu, S. Yang, Y. Xiu, Z. Zhang, C. Assi, C. Yuen, Movable antenna enabled integrated sensing and communication, IEEE Trans. Wirel. Commun. (2025).
[31] H. Qin, W. Chen, Q. Wu, Z. Zhang, Z. Li, N. Cheng, Cramér-Rao bound minimization for movable antenna-assisted multiuser integrated sensing and communications, IEEE Wirel. Commun. Lett. 13 (12) (2024) 3404–3408.
[32] N. Li, P. Wu, B. Ning, L. Zhu, Sum rate maximization for movable antenna enabled uplink NOMA, IEEE Wirel. Commun. Lett. 13 (8) (2024) 2140–2144.
[33] X. He, W. Chen, Q. Wu, X. Zhu, N. Cheng, Movable antenna enhanced NOMA short-packet transmission, IEEE Commun. Lett. 28 (9) (2024) 2196–2200.
[34] Y. Zhou, W. Chen, Q. Wu, X. Zhu, N. Cheng, Movable antenna empowered downlink NOMA systems: Power allocation and antenna position optimization, IEEE Wirel. Commun. Lett. 13 (10) (2024) 2772–2776.
[35] X. Shao, R. Zhang, 6DMA enhanced wireless network with flexible antenna position and rotation: Opportunities and challenges, 2024, arXiv, arXiv:2406.06064.
[36] X. Shi, X. Shao, R. Zhang, Capacity maximization for base station with hybrid fixed and movable antennas, IEEE Wirel. Commun. Lett. (2024).
[37] Lyu B., H. Liu, W. Hong, S. Gong, F. Tian, Primary rate maximization in movable antennas empowered symbiotic radio communications, in: 2024 IEEE 99th Vehicular Technology Conference, VTC2024-Spring, 2024.
[38] G. Hu, Q. Wu, J. Ouyang, K. Xu, Y. Cai, N. Al-Dhahir, Movable-antenna-array-enabled communications with CoMP reception, IEEE Commun. Lett. (2024).
[39] Cheng Z., N. Li, J. Zhu, X. She, C. Ouyang, P. Chen, Enabling secure wireless communications via movable antennas, in: ICASSP 2024-2024 IEEE International Conference on Acoustics, Speech and Signal Processing, ICASSP, 2024.
[40] G. Hu, Q. Wu, K. Xu, J. Si, N. Al-Dhahir, Secure wireless communication via movable-antenna array, IEEE Signal Process. Lett. (2024).
[41] J. Tang, C. Pan, Y. Zhang, H. Ren, K. Wang, Secure MIMO communication relying on movable antennas, IEEE Trans. Commun. (2024).

Pedro Candeias is currently enrolled in the M.Sc. in Electrical and Computer Engineering at Universidade Nova de Lisboa. His academic interests include radio communication systems and networks.

Rodolfo Oliveira received the Licenciatura degree in electrical engineering from the Faculdade de Ciências e Tecnologia (FCT), Universidade Nova de Lisboa (UNL), Lisbon, Portugal, in 2000, the M.Sc. degree in electrical and computer engineering from the Instituto Superior Técnico, Technical University of Lisbon, in 2003, and the Ph.D. degree in electrical engineering from UNL, in 2009. From 2007 to 2008, he was a Visiting Researcher at the University of Thessaly. From 2011 to 2012 and in 2023, he was a Visiting Scholar at Carnegie Mellon University. Rodolfo Oliveira is currently with the Department of Electrical and Computer Engineering, UNL, and is also affiliated as a Senior Researcher with the Instituto de Telecomunicações, where he researches in the areas of Wireless Communications, Computer Networks, and Computer Science. He is currently the Chair of the IEEE Portugal Section and serves on the Editorial Board of Ad Hoc Networks (Elsevier), ITU Journal on Future and Evolving Technologies (ITU J-FET), IEEE Open Journal of the Communications Society, and IEEE Communications Letters.